

Article

Mechanical Assessment in Atherosclerosis Based on Photoacoustic Viscoelasticity Imaging

Xingchao Zhang ¹, Xiaohan Shi ², Hui Wu ¹, Caixun Bai ¹, Junshan Xiu ^{1,*} and Yue Zhao ^{1,*} 

¹ School of Physics and Optoelectronic Engineering, Shandong University of Technology, Zibo 255049, China; xingchaozxc@163.com (X.Z.); wuhui0127@163.com (H.W.); baicaixun@sdut.edu.cn (C.B.)

² School of Mechanical Engineering, Shandong University of Technology, Zibo 255049, China; sxh_edu@126.com

* Correspondence: xiujunshan@sdut.edu.cn (J.X.); zhaoyue@sdut.edu.cn (Y.Z.)

Abstract: Early identification of vulnerable plaques is a major challenge in diagnosis and assessment of atherosclerosis. In atherosclerotic plaque development, the proportion change in components caused plaque mechanical property change and induced plaque rupture. In this paper, a photoacoustic viscoelasticity imaging (PAVEI) technique was proposed to measure the viscosity–elasticity ratio of atherosclerotic plaque and evaluated for the potential in characterizing vulnerable plaques. Apolipoprotein E-knockout mice fed with a high-fat/high-cholesterol diet were chosen as the atherosclerotic model. Plaque component phantoms were examined to demonstrate the high efficiency of PAVEI in detecting the proportion change in components compared to single elasticity or viscosity detection. Finally, atherosclerotic plaques from mice aortas at different stages were imaged by PAVEI, which provided an insight into the compositional and functional characterization of vulnerability plaques and suggested its potential applications in the identification of high-risk plaques.

Keywords: photoacoustic imaging; atherosclerotic plaques; mechanical assessment; viscoelasticity; vulnerability



Citation: Zhang, X.; Shi, X.; Wu, H.; Bai, C.; Xiu, J.; Zhao, Y. Mechanical Assessment in Atherosclerosis Based on Photoacoustic Viscoelasticity Imaging. *Photonics* **2024**, *11*, 471. <https://doi.org/10.3390/photronics11050471>

Received: 15 March 2024

Revised: 5 May 2024

Accepted: 14 May 2024

Published: 17 May 2024



Copyright: © 2024 by the authors. Licensee MDPI, Basel, Switzerland. This article is an open access article distributed under the terms and conditions of the Creative Commons Attribution (CC BY) license (<https://creativecommons.org/licenses/by/4.0/>).

1. Introduction

In recent years, the incidence of cardiovascular and cerebrovascular diseases have increased significantly and become one of the main diseases threatening human health, and the cause of acute cardiovascular disease is mostly plaque rupture after atherosclerosis [1]. Therefore, the early identification of plaques that may rupture has become an important means to actively intervene in the process of cardiovascular and cerebrovascular diseases, and plaque stability has also become an important basis for clinical efficacy evaluation [2]. Pathological studies of atherosclerosis have shown that the process of plaque changing from stable to unstable involves multiple links, such as inflammation, immunity, metabolism and coagulation. There is an inevitable relationship between plaque rupture and the change in plaque mechanical properties. When the ratio of lipids and collagen within the plaque changes, the change in plaque mechanical properties will lead to plaque instability [3]. Most of the diagnostic technology simply showing the morphology of the atherosclerotic tissues can no longer meet the clinical needs. In order to judge the stability of plaques, it is necessary to comprehensively evaluate the morphology and mechanical properties of plaques.

Current studies have shown that elasticity is one of the biomechanical parameters that can reflect the pathological and physiological changes of atherosclerotic tissues [4]. The collagen fibers, smooth muscle and lipid components in the blood vessel wall have regular structure and a strict hierarchy under normal circumstances. In atherosclerosis, changes in the original structure and hierarchy, coupled with the intensification of lipid deposition and inflammatory activity, change the molecular composition and structure of the blood

vessel wall, thus determining the elasticity of the atherosclerotic tissues. Traditional imaging techniques only used elasticity to characterize the mechanical properties of plaques. However, the complexity in mechanical properties of most atherosclerotic tissues could not be fully expressed by the elastic modulus. In the description of viscoelastic characterization and rheological behavior, viscosity is often as important as elasticity. Especially for the vulnerable plaques, elasticity is not enough to describe their complete internal characteristics, so it is necessary to use both viscosity and elasticity to describe the changes in their mechanical characteristics [5,6]. Therefore, the invention of techniques that can accurately assess the viscoelasticity of atherosclerotic plaques is of great significance in the assessment of atherosclerosis and the identification of unstable plaques.

Photoacoustic (PA) techniques, combining the advantages of optical imaging and ultrasound imaging, have made great progress in many biomedical applications in recent years [7–10]. At present, conventional photoacoustic imaging based on tissue light absorption contrast, reflecting the light absorption coefficient of tissue, technically mainly relies on measuring the amplitude of PA signals to invert the light absorption distribution of tissues, and does not consider the viscoelastic information during the process of PA signal generation [11–15]. In fact, when the laser acts on the tissue, according to the photoacoustic effect, the tissue will form thermal expansion vibration, while the viscoelasticity of the tissue will damp the PA generation, and a certain time delay will occur between the laser and the PA signal. Different viscoelastic tissues or pathologies will produce different phase delays under the same excitation conditions; therefore, using the measured phase delay as the imaging contrast, the reconstructed image can reflect the strength of the viscoelasticity in the detection point. Combined with a certain image information processing method, the image reflecting the viscoelastic distribution inside the atherosclerotic tissues can be reconstructed [16,17].

In this paper, a photoacoustic viscoelastic imaging technique was described that can reconstruct different atherosclerotic tissues with high resolution and high contrast. Phantoms mixed with different proportions of lipid and collagen were examined to demonstrate the high efficiency of PAVEI in detecting the change in components compared to single elasticity or viscosity detection. Atherosclerotic tissues from apolipoprotein E-knockout mice aortas at different stages were imaged by PAVEI to accurately assess the viscoelasticity of the plaques, which helps the diagnosis and assessment of cardiovascular and cerebrovascular diseases simultaneously.

2. Principles and Methods

To radiate absorptive isotropic viscoelastic structures, an intensity-modulated continuous wave laser was used. The light intensity can be expressed as $I = \frac{1}{2}I_0(1 + \cos\omega t)$, where ω is the modulation frequency and I_0 is the light intensity. Then sinusoidal temperature variation $T = T_0e^{i\omega t}$ due to the light absorption by the viscoelastic structures will then cause thermal expansion and PA wave generation, and the dominant frequency of the PA wave will be equal to the modulated frequency of the laser with cyclical changes. During the PA generation process, the cyclical temperature variation induces cyclical thermal stress, which causes corresponding strain in the form of cyclical PA waves. Because the viscoelastic structures will damp the above process, the PA wave would be out of phase with the laser.

In a spherical coordinate system, to find the changes in rheological thermal stress caused by a periodic variational point heat source of unbounded isotropic viscoelastic structures, the radial thermal stress can be expressed as:

$$\sigma = -\frac{4G}{r} \frac{\partial \phi}{\partial r} + \rho \frac{\partial^2 \phi}{\partial t^2} \quad (1)$$

where G is the Green's function of thermal conduction, ϕ is defined by $\Delta\phi = \alpha T(1 + \nu)(1 - \nu)$; in the condition of temperature $T = T_0 e^{i\omega t}$, the stress σ becomes:

$$\sigma = -E\alpha T_0 e^{i\omega t} / (1 - \nu) \tag{2}$$

where E is the Young's modulus, α is the coefficient of linear expansion, ω is the modulation frequency, ν is the Poisson's ratio. The differential constitutive equation of viscoelastic structures can be defined as:

$$P\sigma = Q\varepsilon \tag{3}$$

where ε is the strain and the linear differential operator P and Q are defined as $P = \sum_{k=0}^m \frac{d^k}{dt^k}$, $Q = \sum_{k=0}^m q_k \frac{d^k}{dt^k}$. Combining the Equations (2) and (3):

$$\sum_{k=0}^m p_k (i\omega)^k \sigma_0 e^{i\omega t} = \sum_{k=0}^m q_k \frac{d^k \varepsilon}{dt^k} \tag{4}$$

Due to the fact that p_k and q_k are integers, the solution to Equation (4) can be given as $\varepsilon(t) = \varepsilon^* e^{i\omega t}$, where ε^* is the magnitude of the complex strain. Equation (4) can be rewritten as:

$$\varepsilon^* = \frac{\bar{P}(i\omega)}{\bar{Q}(i\omega)} \sigma_0 \tag{5}$$

where $\bar{P}(i\omega)$ and $\bar{Q}(i\omega)$ are expressed as $\bar{P}(i\omega) = \sum_{k=0}^m p_k (i\omega)^k$, $\bar{Q}(i\omega) = \sum_{k=0}^m q_k (i\omega)^k$, and the stress response can be expressed as:

$$\sigma(t) = \frac{\bar{Q}(i\omega)}{\bar{P}(i\omega)} \varepsilon^* e^{i\omega t} = \frac{\bar{Q}(i\omega)}{\bar{P}(i\omega)} \varepsilon(t) \tag{6}$$

Then, the dynamic modulus can be written as:

$$Y^*(i\omega) = Y_1(\omega) + iY_2(\omega) = \frac{\bar{Q}(i\omega)}{\bar{P}(i\omega)} \tag{7}$$

where $Y_1(\omega)$ and $Y_2(\omega)$ are the two parts of $Y^*(i\omega)$ determined by the modulation frequency ω and constants p_k, q_k . Thus, the Equation (7) be obtained using:

$$\varepsilon(t) = [Y^*(i\omega)]^{-1} \sigma(t) = \frac{Y_1(\omega) - iY_2(\omega)}{\sqrt{Y_1^2(\omega) + Y_2^2(\omega)}} \sigma(t) \tag{8}$$

Equation (8) is the constitutive equation of stress–strain relationship for the viscoelastic structures. The magnitude of the complex strain can then be decomposed:

$$\varepsilon^* = \varepsilon' + i\varepsilon'' = \frac{Y_1(\omega) - iY_2(\omega)}{\sqrt{Y_1^2(\omega) + Y_2^2(\omega)}} \sigma_0 \tag{9}$$

Thus,

$$\varepsilon'' / \varepsilon' = Y_2 / Y_1 \tag{10}$$

The strain response can be expressed as:

$$\varepsilon(t) = \varepsilon^* e^{i\omega t} = (\varepsilon' \cos\omega t - \varepsilon'' \sin\omega t) + i(\varepsilon'' \cos\omega t + \varepsilon' \sin\omega t) \tag{11}$$

denoting,

$$\tan\delta = \varepsilon'' / \varepsilon' = Y_2 / Y_1 \tag{12}$$

The strain response becomes:

$$\varepsilon(t) = \frac{\varepsilon'}{\cos\delta} [\cos(\delta + \omega t) + i\sin(\delta + \omega t)] = \varepsilon_A e^{i(\omega t + \delta)} \quad (13)$$

where δ is the phase delay of the corresponding strain and ε_A is the magnitude of the dynamic strain. To describe the creep process under periodic stress changes, a rheological Kelvin–Voigt model was used, and the dynamic modulus can be written as:

$$Y_1 = E, \quad Y_2 = \omega\eta \quad (14)$$

Then the relationship between the phase delay and viscoelasticity becomes:

$$\eta/E = \tan\delta/\omega \quad (15)$$

Finally, by extracting the phase delay of the PA signals, the viscosity–elasticity ratio can be obtained to describe the mechanical properties of the tissues.

The schematic of the PAVEI technique in atherosclerosis detection is shown in Figure 1. The system used an 808 nm fiber-coupled continuous-wave laser as the excitation source. A function generator was used to apply a 4.5 V sinusoidal signal to the electro-optical modulators, which controlled the intensity of continuous wave lasers at 50 KHz and 90% of the modulation depth. A 4× microscope objective (NA = 0.1) then focused the laser onto the samples. By imaging the blade edge, the current system had a lateral resolution of approximately 65 μm (Supplementary Figure S1) and a time-average laser power density of 100 mw/cm² for measuring the sample surface. An ultrasonic transducer with a center frequency of 50 KHz collected the PA signals, a lock-in amplifier pre-amplified the PA signals and then extracted the phase delay, which was analyzed by the computer to obtain the mechanical property of the samples. Through the two-dimensional scanning of the mechanical scanner over the desired area, the photoacoustic viscoelasticity image can be reconstructed. With photoacoustic lock-in measurements, the system had a higher signal-to-noise ratio (Supplementary Figure S2) and a high quality viscoelasticity image can be obtained [18]. Lipids (L5146; Sigma-Aldrich, St. Louis, MO, USA) and type I collagen (C7774; Sigma-Aldrich) were used to mimic the composition of plaques. A different concentration series of Gelatin phantoms were made by mixing different proportions of lipid and collagen. The PA signals of each phantom were taken with a time constant of 30 ms and average times of 100, then the viscosity–elasticity ratio was calculated. This study was approved by the Animal Study Committee of Shandong University of Technology in Zibo, China. A total of 15 apolipoprotein E-knockout mice served as animal models, 12 mice were fed with a high-fat/cholesterol (HFC) diet (97% normal chow, 2% lard and 1% cholesterol) and killed at different stages for PAVEI assessment, with other mice as controls. The aorta was detached from the coronary artery and cut lengthwise for the PAVEI image and then were stained with oil red O staining for histological measurement. The en-face oil red O staining followed the steps below. After PAVEI, the aortic specimen was pretreated with 60% isopropyl alcohol for 10 min and then incubated with 0.6% Oil Red O (Sigma) solution in 60% isopropyl alcohol for 3 h at room temperature. The aortic specimen was then repeatedly washed with 60% isopropyl alcohol, and then repeatedly washed with water for 2 min. Cross-sectional oil red O staining followed the steps below. Aortic specimens were frozen to −22 °C and sectioned with 8 μm step (CM1850, Leica, Wetzlar, Germany). The cryo-sectioning tissues were pretreated with 60% isopropyl alcohol for 5 min and then incubated with 0.6% oil red O solution in 60% isopropyl alcohol for 15 min. Subsequently, tissues were washed in running tap water for 2 min. Finally, tissues were treated with hematoxylin for 1 min to stain the cell nuclei and excess stain was removed by running tap water. All data were analyzed using a *t*-test and were expressed as mean ± SD, *p* values < 0.01 were considered statistically significant [19–23].

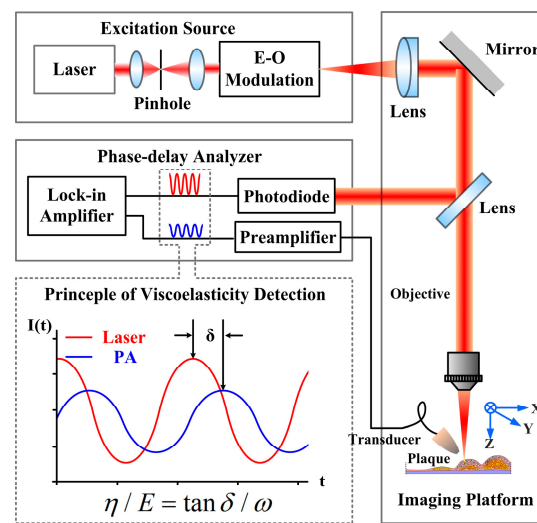


Figure 1. Atherosclerotic tissue was excited with a sinusoidally modulated laser. This process generated a PA signal in the tissue at the same frequency as the excitation but with a delay in the relative phase. Through the recording and analysis of the PA phase delay, the viscoelasticity image of the atherosclerotic plaques could be reconstructed.

3. Results

As the main components in atherosclerotic plaques and leading to fragile plaque rupture, lipids and collagen are directly related to the mechanical property and plaque morphology. Through analysis, PAVEI has a good ability to distinguish plaque components in simulated tissue models composed of different proportions of lipids and collagen. Figure 2 showed the relationship between lipid or collagen content (Figure 2A) and the viscosity–elasticity ratio, and the averaged viscosity–elasticity ratio of phantoms containing different ratios of lipids and collagen; the PAVEI images of the phantoms were also shown in Figure 2B. The accuracy of PAVEI was confirmed through a comparison with rheometers, which were considered the gold standard viscoelastic measurement method (Figure 2C,D). As theoretically predicted, viscosity–elasticity ratio increased with increasing lipids compared to collagen.

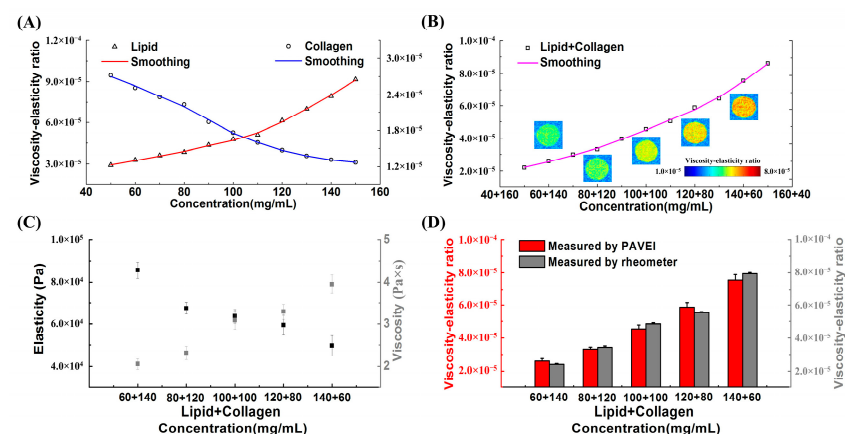


Figure 2. Average viscosity–elasticity ratios of phantoms containing various concentrations of lipid or collagen (A), and of phantoms mixed with different proportions of lipid and collagen (B). (C) Elasticity and viscosity measured by rheometer. (D) Comparison between the viscosity–elasticity ratios measured by PAVEI and rheometer.

To demonstrate the high efficiency of PAVEI in detecting the proportion change in plaque components, we measured the elasticity modulus, viscous coefficients and the

viscosity–elasticity ratio of plaque component phantoms and the fatty plaque from an atherosclerotic tissue. As is evident in Figure 3A, the elasticity modulus and viscous coefficients of the phantoms, which mixed with different proportions of lipid and collagen, were 63.5 kPa, 3.08 Pa·s and 59.4 kPa, 3.28 Pa·s, respectively. The difference in elasticity and viscosity were 6.52% and 6.58%, respectively. However, the difference in the viscosity–elasticity ratio measured by PAVEI can reach 29.30% approximately. Furthermore, we verified the viscosity and elasticity changes in atherosclerotic tissues. Figure 3B showed the rheometer and PAVEI results of a control artery and an atherosclerotic one. In the rheometer measurement, the elasticity modulus and viscous coefficients were 55.6 kPa, 1.18 Pa·s and 43.5 kPa, 1.46 Pa·s, respectively. Thus, the difference in elasticity and viscosity were 21.82% and 23.75%, respectively. However, a 58.54% difference in the viscosity–elasticity ratio can be obtained in PAVEI, much higher than that of single parameter. By comparing the test results of phantoms mixed with different proportions of lipid and collagen, obtained using a rheometer, the change in the different components in the phantoms indeed caused the change in elasticity and viscosity. In the case of little changes in composition, the elastic or viscosity change will be very small. However, the PAVEI technique measured the viscosity–elasticity ratio, which magnified the opposing changes in viscosity and elasticity that occur during atherosclerosis and amplified the mechanical change in the composition, thus enabling a more effective detection of plaque pathology with higher sensitivity and higher contrast.

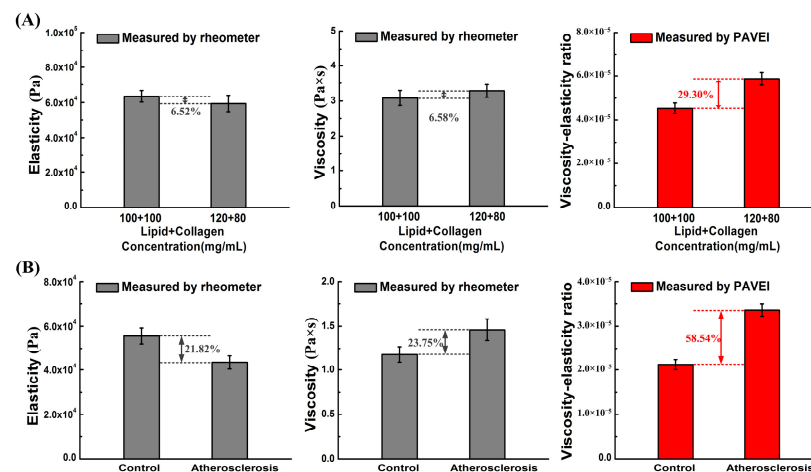


Figure 3. Elasticity and viscosity of (A) phantoms mixed with different proportions of lipid and collagen and (B) the atherosclerotic artery and the control one measured by rheometer, and the viscosity–elasticity ratios measured by PAVEI.

The PAVEI system was capable of characterizing lesions in atherosclerotic plaques (Figure 4). Figure 4A showed a cross-sectional PAVEI for a healthy artery and an atherosclerotic artery. Due to the high viscoelasticity of lipids, atherosclerotic plaques contrasted strongly with the normal arterial wall. Figure 4B showed the oil red O staining results of the arterial samples in Figure 4A, showing the changes in composition of the arteries clearly. The main components of plaques were lipids and collagen. The averaged viscosity–elasticity ratio of the plaque with lipid accumulation was 2.75×10^{-5} which was increased compared to 2.35×10^{-5} from the control group (Figure 4C). A comparison between groups was performed using a *t*-test ($p < 0.01$), which ensured the accuracy of PAVEI in presenting the lipid composition in atherosclerotic plaques. Oil red O was mainly used to stain the lipid region; the different staining degrees represent the lipid content, and the distribution of lipids in plaques can be visually seen through the staining results. The unstained part was mainly composed of collagen fibers, which was an important component in maintaining plaque stability. The correspondence between the PAVEI images and the results of the

histological sections clearly showed that the lipids greatly increased the viscosity–elasticity ratio in the mechanical properties of atherosclerotic tissues.

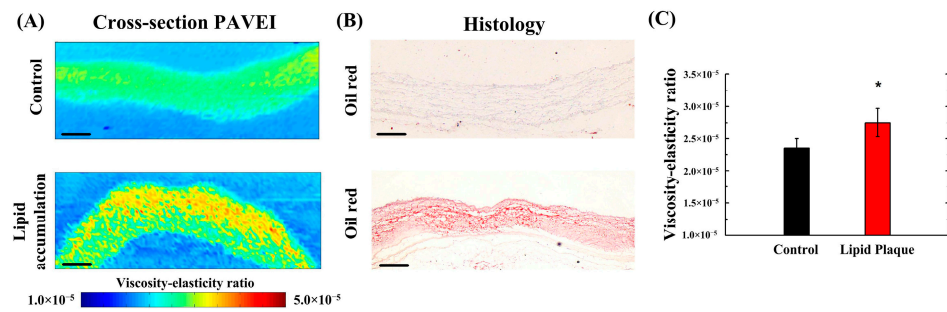


Figure 4. (A) Cross-section PAVEI of the control artery compared to the atherosclerotic one. (B) Corresponding oil red O staining results. Bars = 100 μm . * $p < 0.01$ for lipid plaque group vs control group. (C) Comparison of the viscosity–elasticity ratio measured by PAVEI. * $p < 0.01$ for control artery vs lipid plaque.

Figure 5A was obtained from atherosclerotic plaques found in apolipoprotein E-knockout mice with 4 to 12 weeks of HFC diet. Histological results obtained by oil red O staining showed the changes in lipids on the surface of the vessel lumen during this period (Figure 5B). In the data processing of PAVEI results from the atherosclerosis groups, the viscosity–elasticity ratio of the control group was taken as the threshold value, and then the viscosity–elasticity ratio of the atherosclerotic tissues that was above the threshold was statistically averaged. The plaques in mice 4 weeks into the HFC diet were early lesions with an averaged viscosity–elasticity ratio of 2.64×10^{-5} . The mice after 8 weeks of the HFC diet had significantly more mixed lipids in their vascular walls with an averaged viscosity–elasticity ratio of 2.87×10^{-5} . High-grade fat regions were observed after 12 weeks of the HFC diet, where the viscosity–elasticity ratio ranged from 3.02×10^{-5} to 3.58×10^{-5} , corresponding to an increase in lipid content. The statistical analysis of the high lipid content area measured by PAVEI is shown in Figure 5C, and statistical significance was compared using a *t*-test to identify group differences, resulting in *p* value < 0.01 . The correspondence between histological sections and PAVEI images indicated that lipids produced contrast in PAVEI. This validation ensured that PAVEI can accurately identify lipid accumulation during plaque lesions.

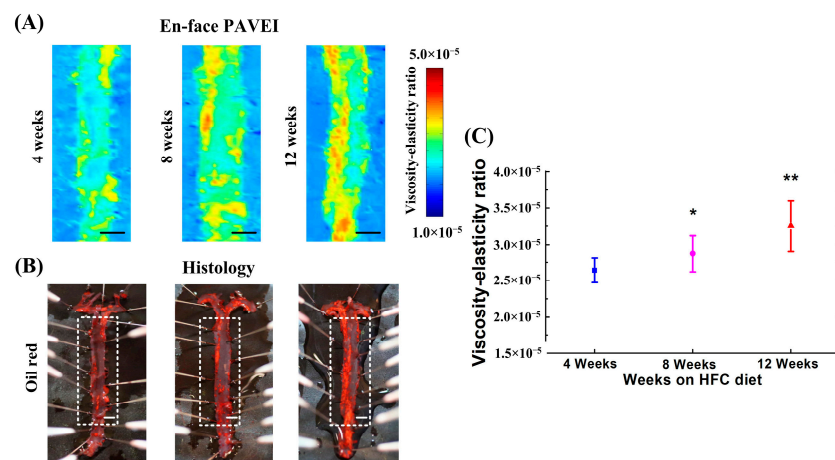


Figure 5. (A) En-face PAVEI and (B) histology acquired from the luminal surface with different duration of HFC diet (4, 8, 12 weeks). The white dashed box showed the imaging area in Figure (A). Bars = 1 mm. (C) Comparison of the viscosity–elasticity ratio measured by PAVEI. * $p < 0.01$ for 8-week group vs 4-week group; ** $p < 0.01$ for 12-week group vs 8-week group.

4. Discussion

One aim of the study was to show the capability of PAVEI to characterize the mechanical properties of atherosclerotic tissue and thus differentiate plaque components. Lipid and collagen played important roles in the development of atherosclerosis, and the change in their proportion will lead to a change in plaque mechanical properties. Lipids were the main component, which were usually covered with a layer of collagen fibers that protected blood vessels and prevented the plaque from rupturing. Early lipid accumulation was only on the surface of blood vessels, and did not make the plaque unstable. With the increase in lipid accumulation, a necrotic lipid core will form and the plaque will become vulnerable. On the other hand, the main component of the fiber cap was collagen; thus, changes in the ratio of lipids to collagen reflected changes in the fiber cap, ultimately leading to changes in plaque stability. In this study, two-dimensional maps of atherosclerotic tissue were reconstructed to evaluate the plaque viscoelasticity. Significantly higher viscosity–elasticity ratios were found in fatty plaques compared to normal arteries. These results indicated that the mean viscosity–elasticity ratio of the plaque was dominated by the tissue type.

Another aim was to determine what composition generates areas with a high viscosity–elasticity ratio, as identified via PAVEI. Therefore, we analyzed cross-sections of atherosclerosis plaques via PAVEI and validated the results with histology. First, there was a significant relationship between the fatty area and the average viscosity–elasticity ratio. Fat-laden macrophages (FLMs) played a big role in the formation of fatty plaques. In the early stage of atherosclerosis, FLMs phagocytized lipids and the fatty area was directly related to the intimal accumulations of numerous FLMs. As atherosclerosis progressed, activated FLMs secreted proteolytic enzymes and matrix metalloproteinases to degrade the fibrous cap, leading to plaque rupture. Therefore, an increase in the amount of accumulated FLMs was often accompanied by an increase in the viscosity–elasticity ratio of plaques [24,25]. Second, there was an inverse correlation between the plaque viscosity–elasticity ratio and the collagen content, which was closely related to the weakening of atherosclerotic plaques at points of rupture. The loss of collagen was the main reason for the increase in plaque vulnerability, and plaques containing less collagen were thought to be more likely to break. Therefore, in our study, the viscosity–elasticity ratio measured using the PAVEI technique can be identified as an important mechanical index to evaluate the vulnerability of plaques. All sections of lesions in this study contained no calcium. However, it is possible that the stiff calcium deposits in plaque increase the propensity to rupture, and that calcification may be a marker for the extent of disease or for another process such as inflammation. Due to the high hardness of calcification, PAVEI will attribute a much lower viscosity–elasticity ratio to calcified areas compared to other pathologies [26–29].

This study had several limitations which should be noted. Due to the low frequency of an ultrasonic transducer in this system, the size of the transducer was big and its radius was about 3 cm, which made it unable to do any in vivo intravascular detection. In the future, a transducer with a low radius or update on detection mode can be used to solve this key problem during the promotion of intravascular PAVEI technique. Because the energy of the continuous laser was relatively weak, the signal-to-noise ratio (SNR) of the excited PA signal in the experiment was relatively poor, thus the PA signals need to be amplified by the lock-in amplifier and then collected by the ultrasound transducer. In the future, a high frequency pulsed laser should be used to greatly improve the SNR of the PA signal, improving the contrast of the PAVEI images and the sensitivity of the system. The step size during the scanning of atherosclerotic tissue was 25 μm . When detecting the system resolution, a blade with high uniformity and flatness was used, thus the resolution results were much better. However, in the detection of atherosclerotic samples, due to the unevenness of the plaques, the focusing effect of the laser on the tissue surface was not good. As a result, the resolution and contrast of the PAVEI image in Figures 4 and 5 were not very good. The atherosclerotic specimens used in ex vivo studies may have degraded, so the measured viscosity–elasticity ratio may change slightly, but differences in mechanical properties between different plaque types should remain under in vivo

conditions in the future. The main reason for the low resolution of the PAVEI images was that the scanned area was very small, and the radius of blood vessels in mice was less than 1 mm, so it is difficult to get a very clear image. In the future, the resolution of PAVEI can be improved by using a high-power objective lens to achieve the high-resolution detection of atherosclerotic plaques.

Possibly the most important factor is that, to describe the mechanical properties of an isotropic material, a minimum of two parameters (i.e., Young's modulus and the coefficient of viscosity) are required. However, biological materials are rarely isotropic, and as a result, more parameters must be defined via further study to describe the complex mechanical behavior of a plaque. Although the viscosity–elasticity ratio reflected the different mechanical behaviors of various types of tissues, further research is needed to separate the elasticity modulus and viscous coefficients, versus the viscoelasticity contributions to the mechanical behavior of atherosclerotic tissues. Our group has been carrying out the research in photoacoustic quantitative elasticity modulus determination. Combined with PAVEI, we can obtain the viscous coefficient of the atherosclerotic tissue, which allows for the multi-parameter detection of plaque pathology and will contribute to a more comprehensive description of plaque vulnerability. Combined with traditional PA imaging, multi-parameter measurements of laser absorption, elasticity, viscosity and viscosity–elasticity ratio can also be realized simultaneously to cooperatively realize the morphological and functional evaluation in atherosclerosis. The detection of the viscosity–elasticity ratio between different plaques has high statistical significance. With the accumulation of large amounts of experimental data, it may be possible to use the PAVEI technique to distinguish different stages of atherosclerotic plaque in the future, and it is also possible to detect other types of vascular diseases through the viscosity–elasticity ratio using the PAVEI technique.

5. Conclusions

In this paper, the PAVEI technique was proposed to evaluate the vulnerability of atherosclerotic plaques using the viscosity–elasticity ratio. The high sensitivity and reliable contrast of the PAVEI system were demonstrated through an analysis of the change in mechanical characteristics caused by the change in composition in gelatin phantoms. In addition, PAVEI can also realize the determination of the mechanical properties of atherosclerotic plaques and differentiate between plaque components, which revealed higher mean viscosity–elasticity ratio values in fatty plaques compared to normal arteries. All the advantages revealed that the PAVEI technique has wide application prospects in detecting the morphological and mechanical characteristics of atherosclerotic plaques.

Supplementary Materials: The following supporting information can be downloaded at: <https://www.mdpi.com/article/10.3390/photonics11050471/s1>. Figure S1: Resolution of the PAVEI system. Figure S2: Amplitude and phase delay of PA signals and noise.

Author Contributions: Conceptualization, X.Z. and Y.Z.; methodology, X.Z.; software, X.S.; validation, H.W. and Y.Z.; formal analysis, X.Z.; investigation, X.S.; resources, H.W.; data curation, X.Z.; writing—original draft preparation, X.Z.; writing—review and editing, Y.Z.; visualization, J.X.; supervision, C.B.; project administration, Y.Z.; funding acquisition, C.B. and J.X. All authors have read and agreed to the published version of the manuscript.

Funding: This work was supported by the National Natural Science Foundation of China (Grant No. 12204279, 12304324); Natural Science Foundation of Shandong Province, China (Grant No. ZR2022MA044).

Institutional Review Board Statement: The animal study protocol was approved by the the Animal Study Committee of Shandong University of Technology in Zibo, China.

Informed Consent Statement: Not applicable.

Data Availability Statement: Data are contained within the article.

Acknowledgments: The authors appreciate Yonggang Lu for his help in data statistical analysis and histological methodologies.

Conflicts of Interest: The authors declare no conflict of interest.

References

- Virmani, R.; Burke, A.P.; Farb, A.; Kolodgie, F.D. Pathology of the Vulnerable Plaque. *J. Am. Coll. Cardiol.* **2006**, *47*, C13–C18. [[CrossRef](#)]
- Fukumoto, Y.; Libby, P.; Rabkin, E.; Hill, C.C.; Enomoto, M.; Hirouchi, Y.; Shiomi, M.; Aikawa, M. Statins Alter Smooth Muscle Cell Accumulation and Collagen Content in Established Atheroma of Watanabe Heritable Hyperlipidemic Rabbits. *Circulation* **2001**, *103*, 993–999. [[CrossRef](#)]
- Maldonado, N.; Kelly-Arnold, A.; Vengrenyuk, Y.; Laudier, D.; Fallon, J.T.; Virmani, R.; Cardoso, L.; Weinbaum, S. A Mechanistic Analysis of the Role of Microcalcifications in Atherosclerotic Plaque Stability: Potential Implications for Plaque Rupture. *Am. J. Physiol. Heart Circ. Physiol.* **2012**, *303*, H619–H628. [[CrossRef](#)] [[PubMed](#)]
- De Korte, C. Morphological and Mechanical Information of Coronary Arteries Obtained with Intravascular Elastography. Feasibility Study in Vivo. *Eur. Heart J.* **2002**, *23*, 405–413. [[CrossRef](#)] [[PubMed](#)]
- Gardner, C.M.; Tan, H.; Hull, E.L.; Lisauskas, J.B.; Sum, S.T.; Meese, T.M.; Jiang, C.; Madden, S.P.; Caplan, J.D.; Burke, A.P.; et al. Detection of Lipid Core Coronary Plaques in Autopsy Specimens With a Novel Catheter-Based Near-Infrared Spectroscopy System. *JACC Cardiovasc. Imaging* **2008**, *1*, 638–648. [[CrossRef](#)] [[PubMed](#)]
- Nair, A.; Kuban, B.D.; Tuzcu, E.M.; Schoenhagen, P.; Nissen, S.E.; Vince, D.G. Coronary Plaque Classification With Intravascular Ultrasound Radiofrequency Data Analysis. *Circulation* **2002**, *106*, 2200–2206. [[CrossRef](#)] [[PubMed](#)]
- Rogowska, J. Optical Coherence Tomographic Elastography Technique for Measuring Deformation and Strain of Atherosclerotic Tissues. *Heart* **2004**, *90*, 556–562. [[CrossRef](#)] [[PubMed](#)]
- Chen, C.; Zhao, Y.; Yang, S.; Xing, D. Integrated Mechanical and Structural Features for Photoacoustic Characterization of Atherosclerosis Using a Quasi-Continuous Laser. *Opt. Express* **2015**, *23*, 17309. [[CrossRef](#)]
- Schaar, J.A.; De Korte, C.L.; Mastik, F.; Strijder, C.; Pasterkamp, G.; Boersma, E.; Serruys, P.W.; Van Der Steen, A.F.W. Characterizing Vulnerable Plaque Features With Intravascular Elastography. *Circulation* **2003**, *108*, 2636–2641. [[CrossRef](#)]
- Yabushita, H.; Bouma, B.E.; Houser, S.L.; Aretz, H.T.; Jang, I.-K.; Schlerdorf, K.H.; Kauffman, C.R.; Shishkov, M.; Kang, D.-H.; Halpern, E.F.; et al. Characterization of Human Atherosclerosis by Optical Coherence Tomography. *Circulation* **2002**, *106*, 1640–1645. [[CrossRef](#)]
- Sethuraman, S.; Amirian, J.H.; Litovsky, S.H.; Smalling, R.W.; Emelianov, S.Y. Spectroscopic Intravascular Photoacoustic Imaging to Differentiate Atherosclerotic Plaques. *Opt. Express* **2008**, *16*, 3362. [[CrossRef](#)] [[PubMed](#)]
- Wang, B.; Yantsen, E.; Larson, T.; Karpiouk, A.B.; Sethuraman, S.; Su, J.L.; Sokolov, K.; Emelianov, S.Y. Plasmonic Intravascular Photoacoustic Imaging for Detection of Macrophages in Atherosclerotic Plaques. *Nano Lett.* **2009**, *9*, 2212–2217. [[CrossRef](#)] [[PubMed](#)]
- Lou, C.; Dai, J.; Wang, Y.; Zhang, Y.; Li, Y.; Liu, X.; Ma, Y. Highly Sensitive Light-Induced Thermoelastic Spectroscopy Oxygen Sensor with Co-Coupling Photoelectric and Thermoelastic Effect of Quartz Tuning Fork. *Photoacoustics* **2023**, *31*, 100515. [[CrossRef](#)] [[PubMed](#)]
- Lou, C.; Dai, J.; Wang, Y.; Zhang, Y.; Li, Y.; Liu, X.; Li, R.; Ma, Y. Quartz Tuning Fork-Based High Sensitive Photodetector by Co-Coupling Photoelectric and the Thermoelastic Effect of Perovskite. *Opt. Express* **2023**, *31*, 10027. [[CrossRef](#)] [[PubMed](#)]
- Bourantas, C.V.; Garcia-Garcia, H.M.; Naka, K.K.; Sakellarios, A.; Athanasiou, L.; Fotiadis, D.I.; Michalis, L.K.; Serruys, P.W. Hybrid Intravascular Imaging. *J. Am. Coll. Cardiol.* **2013**, *61*, 1369–1378. [[CrossRef](#)] [[PubMed](#)]
- Zhao, Y.; Yang, S.; Chen, C.; Xing, D. Simultaneous Optical Absorption and Viscoelasticity Imaging Based on Photoacoustic Lock-in Measurement. *Opt. Lett.* **2014**, *39*, 2565. [[CrossRef](#)] [[PubMed](#)]
- Gao, G.; Yang, S.; Xing, D. Viscoelasticity Imaging of Biological Tissues with Phase-Resolved Photoacoustic Measurement. *Opt. Lett.* **2011**, *36*, 3341. [[CrossRef](#)] [[PubMed](#)]
- Zhao, Y.; Chen, C.; Yang, S.; Xing, D. Mechanical Evaluation of Lipid Accumulation in Atherosclerotic Tissues by Photoacoustic Viscoelasticity Imaging. *Opt. Lett.* **2016**, *41*, 4522. [[CrossRef](#)] [[PubMed](#)]
- Barnes, H.A.; Hutton, J.F.; Walters, K. *An Introduction to Rheology*; Elsevier: Amsterdam, The Netherlands, 1989.
- Junqueira, L.C.U.; Bignolas, G.; Brentani, R.R. Picrosirius Staining plus Polarization Microscopy, a Specific Method for Collagen Detection in Tissue Sections. *Histochem. J.* **1979**, *11*, 447–455. [[CrossRef](#)]
- Aikawa, M.; Rabkin, E.; Okada, Y.; Voglic, S.J.; Clinton, S.K.; Brinckerhoff, C.E.; Sukhova, G.K.; Libby, P. Lipid Lowering by Diet Reduces Matrix Metalloproteinase Activity and Increases Collagen Content of Rabbit Atheroma: A Potential Mechanism of Lesion Stabilization. *Circulation* **1998**, *97*, 2433–2444. [[CrossRef](#)]
- Tekabe, Y.; Li, Q.; Rosario, R.; Sedlar, M.; Majewski, S.; Hudson, B.I.; Einstein, A.J.; Schmidt, A.M.; Johnson, L.L. Development of Receptor for Advanced Glycation End Products-Directed Imaging of Atherosclerotic Plaque in a Murine Model of Spontaneous Atherosclerosis. *Circ. Cardiovasc. Imaging* **2008**, *1*, 212–219. [[CrossRef](#)]
- Zhang, J.; Yang, S.; Ji, X.; Zhou, Q.; Xing, D. Characterization of Lipid-Rich Aortic Plaques by Intravascular Photoacoustic Tomography. *J. Am. Coll. Cardiol.* **2014**, *64*, 385–390. [[CrossRef](#)] [[PubMed](#)]
- Davies, M.J.; Richardson, P.D.; Woolf, N.; Katz, D.R.; Mann, J. Risk of Thrombosis in Human Atherosclerotic Plaques: Role of Extracellular Lipid, Macrophage, and Smooth Muscle Cell Content. *Heart* **1993**, *69*, 377–381. [[CrossRef](#)]

25. Huber, S.A.; Sakkinen, P.; Conze, D.; Hardin, N.; Tracy, R. Interleukin-6 Exacerbates Early Atherosclerosis in Mice. *Arterioscler. Thromb. Vasc. Biol.* **1999**, *19*, 2364–2367. [[CrossRef](#)] [[PubMed](#)]
26. Huang, H.; Virmani, R.; Younis, H.; Burke, A.P.; Kamm, R.D.; Lee, R.T. The Impact of Calcification on the Biomechanical Stability of Atherosclerotic Plaques. *Circulation* **2001**, *103*, 1051–1056. [[CrossRef](#)] [[PubMed](#)]
27. Vengrenyuk, Y.; Carlier, S.; Xanthos, S.; Cardoso, L.; Ganatos, P.; Virmani, R.; Einav, S.; Gilchrist, L.; Weinbaum, S. A Hypothesis for Vulnerable Plaque Rupture Due to Stress-Induced Debonding around Cellular Microcalcifications in Thin Fibrous Caps. *Proc. Natl. Acad. Sci. USA* **2006**, *103*, 14678–14683. [[CrossRef](#)] [[PubMed](#)]
28. Rambhia, S.H.; Liang, X.; Xenos, M.; Alemu, Y.; Maldonado, N.; Kelly, A.; Chakraborti, S.; Weinbaum, S.; Cardoso, L.; Einav, S.; et al. Microcalcifications Increase Coronary Vulnerable Plaque Rupture Potential: A Patient-Based Micro-CT Fluid–Structure Interaction Study. *Ann. Biomed. Eng.* **2012**, *40*, 1443–1454. [[CrossRef](#)]
29. Honda, Y.; Fitzgerald, P.J. Frontiers in Intravascular Imaging Technologies. *Circulation* **2008**, *117*, 2024–2037. [[CrossRef](#)]

Disclaimer/Publisher’s Note: The statements, opinions and data contained in all publications are solely those of the individual author(s) and contributor(s) and not of MDPI and/or the editor(s). MDPI and/or the editor(s) disclaim responsibility for any injury to people or property resulting from any ideas, methods, instructions or products referred to in the content.